WORLD CONFERENCE ON TIMBER ENGINEERING 2025
BRISBANE, AUSTRALIA

Advancing Timber for the Future Built Environment

BENCHMARKING OF A FINITE ELEMENT MODELLING METHODOLOGY FOR TIMBER CONNECTIONS

Juan S. Zambrano-Jaramillo[1], Erica C. Fischer[2]

ABSTRACT: The accurate simulation of timber connections is essential for the advancement of mass timber construction. This study benchmarks finite element modelling methodologies for timber connections using a material model based on continuum damage mechanics. A comparative analysis is conducted between standard and explicit solution methods, utilising previously developed user subroutines available in the literature for analysis in Abaqus. The research evaluates various modelling techniques, assesses numerical instabilities, and identifies best practices for simulating timber connections under different loading conditions. Key factors such as time step selection, contact interactions, and mesh dependency are examined to improve model accuracy and computational efficiency. The study compared the results of timber models using existing subroutines for standard and explicit analysis. Findings indicate that the activation of the crack band method reduced the mesh dependency for elements under tensile stresses; however, from the available user subroutines used for the analysis, the explicit solver exhibited limitations to simulate models where elements experienced stresses in multiple directions and when no localised damage was expected. The research establishes a validated modelling methodology applicable to different material models for both standard and explicit analyses.

KEYWORDS: Finite element analysis, modelling methodology, timber connections, user subroutines.

1 – INTRODUCTION

The global timber market is projected to grow at a compound annual growth rate of 3.39% from 2023 to 2032 [1]. This sustained growth in the timber industry highlights the need for continuous advancements in modelling capabilities to integrate new timber-engineered products into design processes. Furthermore, there is a need for a methodology that simplifies the analysis of timber connections in construction. Timber connections impose complex demands on structural elements due to the combination of tension and shear or compression and shear stresses, which, given the anisotropic nature of timber, often necessitate advanced numerical subroutines for analysis. Consequently, several numerical models have been developed to simulate these connections. However, the lack of consensus among different techniques has resulted in various approaches for simulating timber connections.

Timber as a material can be simulated using the engineering constants of an orthotropic elastic stiffness matrix. However, a more complex model definition is required to consider nonlinear behaviour and simulate damage within the timber (e.g., cracking). A common method used to simulate a timber material is based on continuum damage mechanics [2]. This approach allows the calculation of the material damage produced by the initialisation and expansion of the cracks [3]. Numerically, the nonlinear behaviour of the material is provided by modifying the stiffness matrix when a stress threshold parameter is exceeded, indicating the beginning of the damage. For the simulation, a set of parameters is required to describe the stress-strain relationship of the constitutive model used in the subroutine for each orientation in the timber material. These parameters require previous calibration based on experimental tests of timber specimens to define the mechanical properties [4].

The objectives of this paper are to (i) identify the modelling techniques used to simulate timber connections with material models based on continuum damage mechanics, (ii) compare the results of timber models using the existing Sandhaas [5], [6] subroutines for standard and explicit analysis, and (iii) define a modelling methodology to simulate mass timber connections using previously developed user subroutines. The authors will evaluate the effectiveness and accuracy of different techniques reported in the literature to simulate mass timber connections. The results of this evaluation are to define and generalise the modelling methodology applicable to other material models in future studies. The reported examples used to

[1] Juan Zambrano-Jaramillo, School of Civil and Construction Engineering, Oregon State University, Corvallis, United States, zambraju@oregonstate.edu

[2] Erica Fischer, School of Civil and Construction Engineering, Oregon State University, Corvallis, United States, erica.fischer@oregonstate.edu

https://doi.org/10.52202/080513-0049

compare the finite element models (FEMs) with both subroutines were previously validated in the literature [7].

2 – BACKGROUND

Timber is an anisotropic material, and its most general classification is based on the alignment of the element fibres. The main orientation is parallel to the grain, also known as the longitudinal direction. The secondary orientation includes two directions, both perpendicular to the grain, identified as the radial and tangential directions. Each orientation can fail independently, with ductile compression behaviour and brittle failure in tension and shear. Various approaches have been developed to replicate these failure patterns and create numerical models that simulate timber behaviour. These approaches are typically implemented in FEM to simplify the analysis process and quantify potential damage in timber elements.

Jayasekara and Foster [6] provided a summary of different failure criteria for timber materials. Each approach considers different yield surfaces to trigger the damage parameters that modify the material stiffness and, consequently, the residual strength. To measure the level of damage, each stress component or a combination of them is associated with different failure modes. Each material model defines the available failure modes based on the level of detail required to simulate the timber and accurately replicate different experimental tests.

Numerous constitutive models for timber have been designed for analysis in Abaqus, each based on different failure criteria and incorporating continuum damage mechanics (CDM) to simulate material failure. Sandhaas [5] developed a model for standard analysis that describes different failure modes for timber materials. This model includes tension and compression parallel to the grain (longitudinal direction) and tension and compression perpendicular to the grain, combined with shear in the radial and tangential directions. The failure criteria trigger damage once the normalised stress or the sum of the normalised stresses exceeds one. Each stress component is normalised using the corresponding material strength in its specific direction. A detailed discussion of the constitutive model is available in [7]. This model accounts for elastoplastic behaviour in compression and a brittle linear softening response in tension and shear.

Gharib et al. [8] proposed a multilinear material model for each stress component. It includes an initial elastic region, followed by linear hardening and subsequent bi-linear softening, adjustable for various purposes. This general model was simplified to an elastoplastic model with isotropic hardening for compression perpendicular to the grain and perfect plastic behaviour parallel to the grain. Additionally, it follows conventional linear softening behaviour for brittle failure in tension and shear.

Wang et al. [9] maintained the elastoplastic behaviour from Sandhaas's model for compression and investigated three damage models for tension and shear. An exponential degradation model was introduced to evaluate wood deformation and stiffness degradation under cyclic longitudinal compression. Eslami et al. [10] adopted the Hoffman [11] criteria to maintain the material model's anisotropic yield behaviour. Strain hardening was introduced, and the Hoffman failure criterion was modified to incorporate material strength as a function of plastic strain. This model was validated using three experimental bending tests and additional compression and tension tests from the literature.

Seeber et al. [12] focused his efforts on the compression and tension behaviour of timber, assuming elastoplastic behaviour in compression and brittle softening in tension, similar to other studies. This study included numerical and experimental tests to validate the material in tension and compression in all three directions. All the material models discussed were implemented as UMAT subroutines for standard analysis in Abaqus.

For explicit analysis, Khelifa et al. [13] developed a model to simulate damage in dowel connections within timber structures. This model considered orthotropic elastoplastic behaviour with isotropic hardening and ductile damage, typically associated with wood crushing, metallic dowel yielding, or a combination of both. A VUMAT subroutine was implemented and validated against experimental tests from the literature.

Jayasekara and Foster [6] conducted a comprehensive study analysing the Hill [14] and Hoffman [11] yield criterion combined with the Sandhaas [5] and Gharib et al. [8] models to represent their yield and failure surfaces. The Sandhaas [5] and Gharib et al. [8] implementations were modified to generate a VUMAT subroutine for explicit analysis. In addition, they proposed a composite Hill-Gharib model and a Hoffman-Gharib model, combining the respective yielding criteria with the isotropic hardening and brittle failure defined by the Gharib et al. model. These models were validated using a T-shaped aluminium beam-column connector with bolts and dowels, effectively simulating the ductile yielding and brittle fracture behaviour of timber in the connection model.

The use of FEM in engineering offers an optimal alternative to costly and time-consuming laboratory testing, supporting the introduction of new products and the development of design methodologies [15]. The application of FEM for timber connections has been increasingly growing parallel to the improvements in computational development. In addition to the complex force interactions within connections, damage within timber connections often impacts the overall stiffness of the structure. Therefore, the FEM of timber connections requires detailed damage parameters for both orientations of the timber in addition to simulating the interactions of components within the connection (e.g., between members and dowels).

Material properties

For isotropic or orthotropic materials, FEMs can simulate performance under multidirectional loads. However, timber's anisotropic and nonlinear behaviour adds complexity, leading to numerical instabilities and increased computational demands. Sandhaas [5] reported that the material model was capable of simulating initial nonlinear behaviour in joints caused by the crushing of the timber fibres and the stiffness reduction in perpendicular directions.

 https://doi.org/10.52202/080513-0049

The material model was defined as a nonlinear anisotropic material, considering timber damage in each direction using continuum damage mechanics principles. Sandhaas [5] developed a user subroutine for FEM in Abaqus that requires a set of 18 input parameters to define the linear and nonlinear material behaviour. As described before, the constitutive rule specifies ductile elastoplastic behaviour for compression, both parallel and perpendicular to the grain, and brittle softening for tension and shear stresses.

Step iterations

Standard and explicit solution methods in Abaqus use the large displacement theory. The step iteration size depends on the solver used, affecting the material model's increment size dependency. For standard analysis, increment sizes range from 0.0001 to 0.1. Larger steps may cause overestimation or early failure of elements. Sandhaas [7] recommends a maximum increment of 0.001 to minimise the errors, though it results in a computationally expensive solution. The same author also provided additional analysis related to the influence of the time steps assigned for standard analyses.

In explicit analysis, increment size is controlled by the loading rate and automatically adjusted for model stability. However, to avoid dynamic effects and replicate a pseudo-static procedure, mass scaling has been used to control the time increment of the solver or automatically modify the mass of the elements to control the kinetic energy of the model [16]. For both analysis methods, setting a small first iteration is recommended to allow the model to fit all the interactions and iteratively identify the maximum allowed step size to balance efficiency and accuracy.

Contact interactions

The connections of structural elements involve the interaction between a variety of elements and materials. To simulate these contact interactions between the element surfaces, the general contact algorithm was selected. In the normal direction, hard contact was considered, while the tangential behaviour was defined by the penalty method with a friction coefficient of 0.3 for contact between two steel parts and 0.5 for contact between steel and timber parts [7]. Other numerical models for timber used similar friction coefficients ranging between 0.2 to 0.5 for the penalty method [6], [9], [17], [18].

Other approaches that were considered in this methodology to simulate the contact between steel and timber materials include variations in the contact definitions. [6] and [19] used the penalty constraint enforcement method and a pressure-overclosure relationship to simulate the contact regions where previous damage to the surface of the timber was considered due to drilling or other procedures. Similarly, with the objective of improving the numerical solution, the augmented Lagrangian method was used to enforce the contact between adjacent surfaces [17].

Mesh dependency

Similar to other FEMs, the mesh size used for the elements is an important parameter for continuum damage mechanics problems. Once the problem becomes nonlinear with a softening behaviour, where at least one element reaches the maximum stress, the stiffness matrix is no longer positive definite. A bifurcation problem starts, having two possible outcomes. For the first case, the solution follows the stress-strain curve, increasing the strains and decreasing the stresses. For the second case, the strain and stresses start to decrease by following the secant stiffness back to the origin [17]. In terms of energy, the solution algorithm will try to dissipate the least amount of energy, leading to a localisation effect where a few elements will increase their strains while the rest will unload through the secant stiffness. Considering the element size, for smaller elements, the softening curve would be closer to the elastic secant unloading.

To reduce the mesh dependency, the element length "h", corresponding to the characteristic element size (smallest element from the FE model), is used to modify the fracture energy "G_f" and express it as a function of the element size.

$$g_f = G_f / h \tag{1}$$

The fracture energy is a mesh-dependent parameter. However, the new characteristic fracture energy "g_f" (1) reduces such mesh-dependency. Therefore, in a coarse mesh, "h" should be large, leading to a smaller characteristic fracture energy, and in a finer mesh, a small "h" should produce a larger characteristic fracture energy to compensate for the amount of energy from smaller elements. This regularisation parameter, also called the crack band method, should be used only for cases where a single failure mode dominates the behaviour, and a localisation effect might occur [7].

To replicate the available results and simulate the timber elements with the subroutine, the finite elements must be defined as 3D brick elements with full numerical integration (C3D8) for the standard analysis, and the explicit analysis, 3D brick elements with reduced integration (C3D8R) can be used.

To define a material model for timber, new user subroutines have been developed to improve the performance and include additional functionalities. Some of the improvements are the incorporation of element deletion [17], new stress-strain relationships to consider timber hardening effect with a softening branch after the ultimate strength [8] and these subroutines have been implemented to perform explicit analysis in Abaqus [6]. The current modelling methodology was evaluated with the user subroutine developed by Sandhaas [5] for standard analysis; however, it applies to the other material models. In addition, the modified Sandhaas subroutine for explicit analysis developed by Jayasekara and Foster [6] was incorporated to compare the results from both subroutines based on the same input variables and numerical models reported in previous research [7].

3 – VALIDATION OF MODELLING METHODOLOGY

Previous studies [7] performed experimental testing and numerical analyses to calibrate a numerical model capable of simulating the behaviour of timber elements exposed to diverse loading conditions. Connections constitute an essential part of a structural system because they are subjected to stresses in multiple directions and their

https://doi.org/10.52202/080513-0049

combinations. The complexity during the analysis of a timber connection relies on the capacity to capture the effect of different stresses over the connection region. Therefore, the numerical models should be capable of replicating those conditions to reduce the uncertainty level of the numerical analysis. At the same time, the models could be used to perform parametric modifications during the design process.

Different FEMs were simulated to validate the numerical modelling methodology and identify a suitable approach for simulating mass timber elements and their interactions between different materials. All cases shown in the next subsections have been reported in previous research [7]. The numerical models were simulated and evaluated in Abaqus using the provided user subroutines that were developed for standard (UMAT) [5] and explicit (VUMAT) [6] analysis, respectively. Table 1 describes the objective for each example and defines the variables of interest used for the comparison. Each of these subroutines requires significant input in the material definition (18 input variables for UMAT and VUMAT). However, depending upon the damage mechanisms within the model and loading definitions, some of the input material properties are more important than others and therefore, the model output is more sensitive to small variations of the input parameters. Each one of these case studies will explore these input parameters to demonstrate and provide guidance to engineers and researchers on the importance of the input parameters given the desired modelling objective.

Table 1: Objectives for the validation cases

Case	Objective	Variables
Beam in tension	Test the material with expected localised damage.	Mesh size, crack band method
Monotonic loading	Test the material without expected localised damage.	Mesh size, crack band method
Compression at different angles	Evaluate different orientations of the material.	Orientation angle
Embedment models	Assess the influence of the material input parameters.	Mesh size, damage threshold, fracture energy

The mesh and the configuration of the models used for the analyses correspond to the same parameters reported in the literature [7]. The response obtained from both user subroutines was compared for each model described in the next sections. The same or equivalent configurations were applied to each model for standard and explicit analysis. The only parameters iterated to identify the values that produced the most accurate response were the output interval and the loading rate for explicit analysis.

The material properties used for the model validation of spruce are provided in Table 2. The material must be defined with 35 solution-dependent state variables (SDV) for standard analysis and 51 SDV for explicit. These variables are required for the material model to track the damage evolution in each orientation. For dynamic analyses, the density of the material should also be provided. The mean density for spruce from test specimens was 445 kg/m3. The Poisson ratio in all directions was assumed to be zero [7].

Statistical analysis

The difference between the capacity curves obtained with standard and explicit solution methods was quantitatively evaluated by calculating the strain energy of each case. The area under the curve (AUC) was calculated with numerical integration using the trapezoid method. In addition, the root mean square error (RMSE) was computed for the embedment tests to estimate the parametric analysis error quantitatively. The RMSE was selected because it can be used as a direct measure of the average difference between the capacity curves for model comparison [20]. All parametric cases from the embedment tests were interpolated with the default case displacement as the objective function to eliminate errors related to the displacement interval.

Table 2: General properties for timber validation

Parameter	Spruce [7]	Units
E_{11}	11000	MPa
$E_{22} = E_{33}$	370	
$G_{12} = G_{13}$	690	
G_{23}	50	
$f_{c,0}$	36	
$f_{t,0}$	24	
$f_{c,90}$	4.3	
$f_{t,90}$	0.7	
f_v	6.9	
f_{roll}	0.5	
$G_{f,t0}$	6	N/mm
$G_{f,t90}$	0.5	
$G_{f,v}$	1.2	
G_{froll}	0.6	
η	0.0001	-

3.1 BEAM IN TENSION

A beam element in tension parallel to the grain was simulated to evaluate the influence of the crack band method and the mesh dependency when localised damage is expected. A reduced tension capacity parallel to the grain (23 MPa instead of 24 MPa) was assigned to one slice of elements to generate a region for localised damage. The model consists of a section 1 mm x 1 mm, 10 mm long. The mesh used for the analysis was 10, 80, and 640 brick elements, as illustrated in Figure 1. Boundary conditions were applied at the beam ends, with full displacement restraints on one side and tension applied to the opposite face of the beam with displacement control. The model was tested with and without the crack band method. For the standard analysis, the viscous regularisation method remained enabled because it provides numerical stabilisation to the numerical solution [7]; the explicit version does not require this regularisation procedure [6].

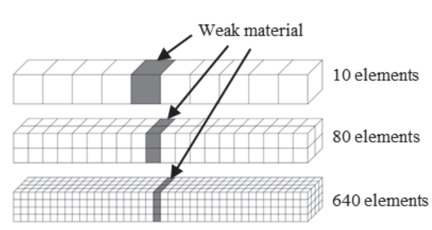

Figure 1. Mesh refinement for beam in tension.

https://doi.org/10.52202/080513-0049

3.2 MONOTONIC LOADING

A series of numerical models with varying mesh sizes were used to evaluate the material response under monotonic loading parallel to the grain. Material properties from Table 2 were uniformly assigned to the model. The effect of the crack band method was examined under conditions where localisation was not expected. Initially, the crack band method was deactivated, as no localisation was anticipated. For comparison, it was later activated for the same cases where loading was applied parallel to the grain to assess its numerical influence.

The analysis was performed on a single cubic element with a side length of 1 mm. The numerical models used to evaluate the material properties were analysed with three different mesh sizes: one, eight, and 125 elements, as illustrated in Figure 2. The analysis was conducted under displacement control and applied to the corresponding face of the cube in the orientation parallel to the grain. Tension was considered as positive displacement, while compression was considered negative displacement.

Figure 2. Mesh refinement for monotonic load evaluation

3.3 COMPRESSION AT DIFFERENT ANGLES TO THE GRAIN

A model was evaluated under monotonic compression, where the local axes were rotated to simulate the timber's orientation at different angles: 0°, 22.5°, 45°, and 90° relative to the longitudinal direction. The crack band method was activated for these cases to capture localised damage. The model consisted of a 40 mm cube located between two steel plates to ensure uniform displacement application (Figure 3). The contact between the steel plates and the cube's faces was defined as hard contact in the normal direction and a penalty coefficient of 0.5 in the tangential direction. The mesh comprised 512 brick elements for the timber cube, while the steel plates were meshed with a similar element size. The applied displacement was oriented normal to the steel plates. Timber material properties were assigned as detailed in Table 2, while the steel plates were modelled as elastic.

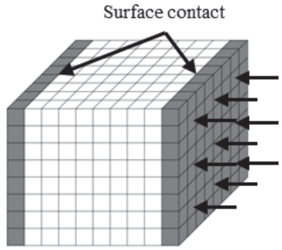

Figure 3. Model configuration for compression tests.

3.4 EMBEDMENT MODELS

An embedment test was modelled to consider the interaction between timber and a steel dowel. Symmetry was applied, reducing the model to a quarter of its actual size. The embedment region was divided into two parts to assign different timber material models: the external region was modelled as an elastic orthotropic material, while the internal region used the constitutive material to capture damage in the timber in contact with the dowel. The numerical model dimensions are provided in Figure 4. Due to the symmetry conditions, half of the 24 mm dowel was included at the bottom centre. The dowel was modelled in direct contact with the timber, with hard contact assigned in the normal direction and a penalty coefficient of 0.5 in the tangential direction. The mesh configuration and its variations are detailed in [7]. Default material properties are listed in Table 2, with a modified fracture energy parallel to the grain of 60 N/mm.

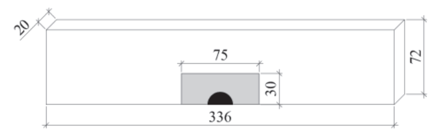

Figure 4. Dimensions for embedment model

To validate the modelling methodology, a parametric analysis was conducted to evaluate the influence of input parameters on the material model and assess changes in the model response due to variations in material properties. For each case, the parameters were independently modified as described in Table 3. The analysis considered variations in mesh size, damage threshold parameters, fracture energy parallel to the grain, fracture energy perpendicular to the grain, and shear fracture energy.

Table 3: Modified material parameters

Parameters	Case
Mesh	Fine
	Coarse
Damage threshold	Threshold = 0.99
	Threshold = 0.80
Fracture energy	$G_{f,t0} = 6$
	$G_{f,t90} = 0.05$ and $G_{f,v} = 0.12$

4 – RESULTS AND DISCUSSION

The reported cases were developed following the methodology described in the previous sections. Standard and explicit analyses were used for their evaluation to compare the differences related to the solution method in addition to the objective provided in Table 1. The configuration applied to the numerical models was equivalent for both solution methods. The results obtained are described for each case defined in the previous section. In all the plots that are shown within this section, "UMAT" refers to a subroutine implemented within the standard solver of Abaqus and "VUMAT" refers to a subroutine implemented within the explicit solver of Abaqus. Additionally, in all the tables used to compare the effect of the crack band method, "NCBM" refers to the cases where the crack band method was not activated and "CBM" refers

https://doi.org/10.52202/080513-0049

to the case when the crack band method was activated for the analysis.

4.1 Beam in tension

The analysis of a beam in tension demonstrated the effect of the crack band method and its relationship with the mesh size when a localised damage region was artificially introduced by reducing the material strength. When the crack band method was deactivated, a mesh-dependent response was observed (Figure 5a), where the finer mesh resulted in a 72% reduction in strain energy compared to the coarser mesh case. In contrast, when the crack band method was activated (Figure 5b), mesh dependency was minimised. However, the solution method significantly influenced numerical stability. In NCBM cases, both solution methods converged similarly up to a displacement of 0.5 mm. For CBM cases with a finer mesh, the UMAT solution experienced convergence issues before reaching 0.4 mm displacement, while the VUMAT solution failed to converge entirely.

Table 4 quantifies the variation in strain energy as a function of the crack band method and mesh size. Negative and positive values indicate the reduction or increase in strain energy relative to the coarser mesh cases. The strain energy was computed as the average of both solution methods, as the response remained unchanged regardless of the subroutine used. The reduction in the AUC for the CBM with finner mesh is related to a lower ultimate displacement compared to the reference model.

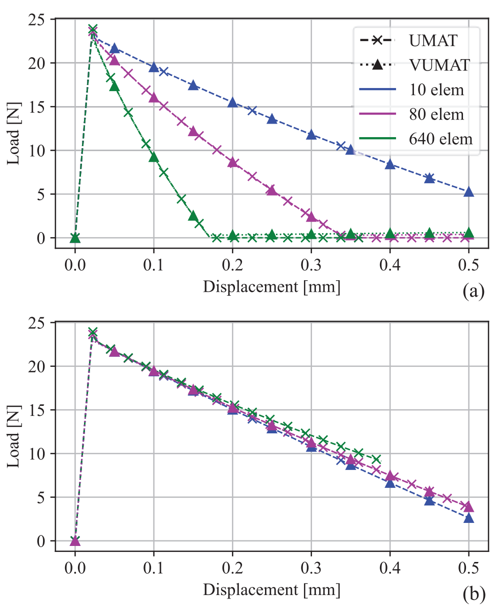

Figure 5. Tension in beam a) without crack band method, and b) with crack band method.

Table 4: Change of strain energy as a function of the mesh size

Mesh [No. elem]	AUC NCBM [%]	AUC CBM [%]
10	Ref.	Ref.
80	-46%	3%
640	-72%	-4%

Ref. = Reference value of AUC per column

4.2 Monotonic loading

The monotonic loading test was used to evaluate the material behaviour without localised damage and to further assess the effect of the crack band method as a function of the mesh size, but this time under tensile and compressive loads. The same material properties were uniformly assigned to the entire model in contrast to section 4.1 where a reduced tension strength was assigned to a single layer to concentrate the damage artificially. The response under compressive loads was not influenced by the crack band method, remaining identical across all cases, regardless of the subroutine or mesh size. In contrast, under tensile loads with the absence of a localised damage region, the deactivation of the crack band method significantly affected the response.

When the crack band method was deactivated, a mesh-dependent response was observed (Figure 6a), where finer meshes resulted in a reduction of strain energy, similar to the beam in tension. The coarser mesh produced a consistent response for both solution methods, while finer meshes introduced additional differences related to the solution approach. In NCBM cases with intermediate mesh sizes, the area under the curve (AUC) decreased by 42% and 47% for the UMAT and VUMAT solutions, respectively. When the crack band method was activated, mesh dependency was significantly reduced (Figure 6b), with AUC variations decreasing to 11% and 4% for the UMAT and VUMAT cases with intermediate mesh sizes. In addition to the visual representation in Figure 6 (a) and (b), Table 5 presents a comparison of strain energy variation in tension between the solution methods. The VUMAT case with a finer mesh exhibited a greater strain energy reduction due to faster softening and earlier strength loss compared to the UMAT case. However, when the crack band method was activated, the VUMAT solutions showed only minor differences, resulting in a more uniform response. Overall, the key finding was that activating the crack band method significantly reduced mesh dependency in the FEM, enhancing the consistency of numerical results.

Table 5: Change of strain energy in tension as a function of the mesh size for each subroutine

Mesh	AUC NCBM		AUC CBM	
[No. elem]	UMAT [%]	VUMAT [%]	UMAT [%]	VUMAT [%]
10	Ref.	Ref.	Ref.	Ref.
80	-42%	-47%	11%	4%
640	-70%	-88%	26%	13%

Ref. = Reference value of AUC per column

https://doi.org/10.52202/080513-0049

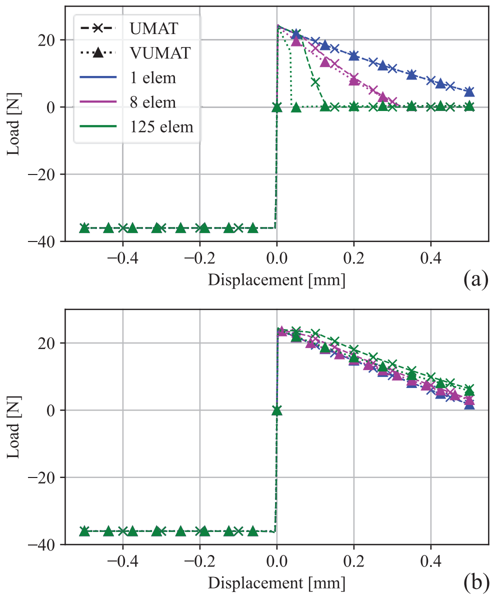

Figure 6. Monotonic load parallel to the grain a) without crack band method, and b) with crack band method.

4.3 COMPRESSION AT DIFFERENT ANGLES TO THE GRAIN

Different rotation angles were applied to the longitudinal direction of the finite element material model to evaluate its influence under compressive loads. Figure 8 presents the load-displacement responses for each solution method and material orientation. Based on the material properties in Table 2, the highest compression capacity was expected parallel to the grain, with a gradual reduction as the rotation angle increased, reaching the lowest compression capacity at 90º (perpendicular to the grain). The results confirmed this expected reduction in compression strength with increasing rotation angles; however, the plastic behaviour differed for the intermediate angles.

Table 6 provides a comparison of the AUC for both solution methods, along with the strain energy ratio between the explicit (VUMAT) and standard (UMAT) solutions, to quantify their similarity. The cases with compression parallel (0º) and perpendicular (90º) to the grain exhibited plastic behaviour after reaching their respective maximum stress values. Additionally, both solution methods produced similar responses, with similar ratios of 99.7% and 98.3%, respectively. In contrast, the intermediate rotation angles (22.5º and 45º) exhibited a more brittle behaviour, differing from the plastic response observed in the principal orientations. This behaviour was attributed to the combined effects of shear and tensile stresses, which induced brittle softening in the material model based on the constitutive definition of the timber material.

The difference between solution methods for these intermediate angles was further quantified in Table 7. The VUMAT solution showed a reduction in strain energy compared to the UMAT solution, with similarity ratios of 67.2% for 22.5º and 16.3% for 45º. This discrepancy was associated with numerical instabilities in the explicit solver, where the timber material model exhibited rapid damage progression due to tensile and shear stresses, leading to the generation of kinetic energy and, consequently, inaccurate results. A similar phenomenon was observed by [5].

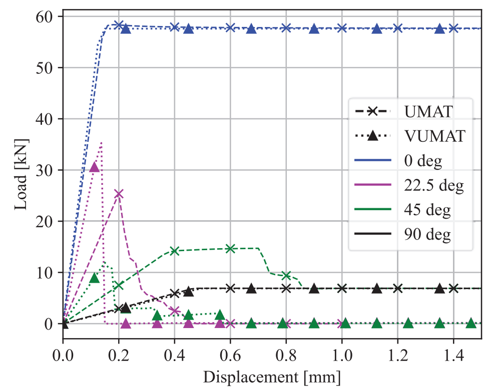

Figure 7. Compression with different angles to the grain.

Table 6: Strain energy relation for both subroutines

Angle [º]	AUC UMAT [J]	AUC VUMAT [J]	Ratio V/U [%]
0	81.36	81.13	99.7%
22.5	4.36	2.93	67.2%
45	13.21	2.15	16.3%
90	8.59	8.45	98.3%

4.4 EMBEDMENT MODELS

An embedment test was modelled to evaluate the interaction between timber and a steel dowel. A default case was established and used as a reference for assessing the influence of material input parameters through a parametric analysis. Before conducting the analysis, the default case was evaluated with and without the crack band method, revealing a 2% difference in the AUC between the models. As suggested by [7], the crack band method was deactivated, as no localisation was expected. The embedment strength was then computed from the numerical models and plotted against dowel displacement for each case (Figure 8). Both solution methods were employed to compare the performance of each subroutine and the material model's sensitivity to variations in the input parameters provided in Table 3.

To assess the behaviour and quantify the response of each model, Table 7 presents the percentage increase or reduction of the AUC for all cases, using the strain energy of the default model with the standard solver as a reference. Additionally, the RMSE was computed for each model relative to the corresponding default case of each solution method (Table 7). This measure was used to determine the mean error in embedment strength, providing a more accurate evaluation of the influence of each modified parameter.

Mesh size influence

Examining the cases with the standard solver (UMAT) in Table 7, a finer mesh resulted in a reduction in strain energy. This reduction was primarily attributed to a lower ultimate displacement (Figure 8b), along with a peak load 6.8% lower than the default case. In contrast, the coarse mesh produced an increase in strain energy compared to the default case. The peak strength increased by 0.6%, while the displacement before strength loss increased, as illustrated in Figure 8c. Regarding the RMSE, both mesh cases exhibited similar values, confirming that the model was sensitive to mesh size, consistent with previous examples where the crack band method was deactivated (sections 4.2 and 4.3).

Effect of damage threshold parameters

The damage threshold parameters were directly modified in the subroutines to assess their influence. When the damage variable approached one, it indicated that total material failure had occurred, leading to zero residual strength. The damage threshold was set to values below one to prevent numerical instabilities. During the parametric analysis, the embedment model was tested with threshold values reduced to 0.99 and 0.80. (Default threshold = 0.9999995 [7]). As shown in Figure 8d and Figure 8e, the residual strength of the material increased, resulting in a higher AUC. For the threshold of 0.80, the embedment strength continued to increase, producing the largest differences in AUC and RMSE values.

Influence of fracture energy

For the fracture energy study, the parameters were reduced to 10% of their values in the default model. This reduction was based on the understanding that fracture energies are the primary calibration parameters of the models [7]. Therefore, the rest of the material properties remained unchanged. In the case of fracture energy for tension parallel to the grain in the standard solver, the AUC decreased by 6%, though this was primarily associated with convergence issues at the end of the analysis (Figure 8f). Regarding the RMSE, this case exhibited the smallest difference from the default case. The fracture energy for tension parallel to the grain had minimal sensitivity to embedment strength, as the damage was primarily caused by fibre crushing in compression, with some elements experiencing tension perpendicular to the grain and shear due to dowel displacement.

For fracture energies related to tension perpendicular to the grain and shear, the effect on AUC was minimal, as well as the case for RMSE in the UMAT solution. These parameters were not directly linked to the primary failure mode of compression parallel to the grain; however, their variation influenced shear failure and tension perpendicular to the grain in elements around the contact region, modifying the embedment response shape, as shown in Figure 8g.

Comparison between solution methods

Overall, the explicit solver was unable to provide a reliable approximation for the embedment model compared to the standard solver. The differences observed in in Figure 8 for the explicit solver suggest early material failure, likely due to the combined effects of stresses in different directions. All cases with the explicit solver exhibited significant variations in AUC relative to the default model. To assess parameter sensitivity within the explicit solver, the RMSE was computed relative to the default explicit model. The fracture energy variation for tension perpendicular to the grain and shear in the explicit solver (Figure 8g) exhibited a closer response to the default case, suggesting that the explicit solver's behaviour was primarily governed by failure in tension perpendicular to the grain and shear stresses.

Table 7: AUC and RMSE of parametric embedment tests

	Parameter	AUC UMAT [%]	AUC VUMAT [%]	RMSE UMAT [kN]	RMSE VUMAT [kN]
(a)	Default	Ref.	-69%	$Ref._U$	$Ref._V$
(b)	Fine mesh	-26%	-58%	4.78	4.62
(c)	Coarse mesh	18%	-38%	6.72	5.80
(d)	Dam. threshold = 0.99	92%	72%	12.76	19.22
(e)	Dam. threshold = 0.80	756%	646%	111.77	103.68
(f)	$G_{f,t0}$ = 6	-6%	-37%	0.07	5.12
(g)	$G_{f,t90}$ = 0.05; $G_{f,v}$ = 0.12	-4%	72%	2.43	18.89

Ref. = Reference value of AUC

$Ref._{U,V}$ = Reference value of RMSE for UMAT and VUMAT cases.

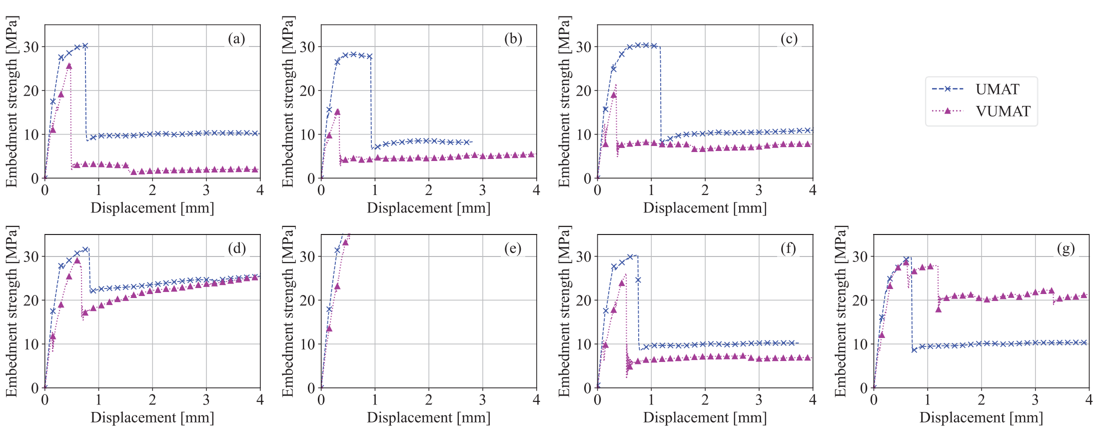

Figure 8. Embedment model a) default case, b) fine mesh, c) coarse mesh, d) small damage threshold reduction, e) large damage threshold reduction, f) reduction of the fracture energy parallel to the grain, and g) reduction of the fracture energy perpendicular to the grain and shear fracture energy.

https://doi.org/10.52202/080513-0049

5 – CONCLUSION

This paper evaluated modelling techniques from the literature used to simulate timber connections based on continuum damage mechanics. Several material models were analysed to identify different approaches for simulating timber connections. Each example provided different failure modes to evaluate the influence of the input parameters. Additionally, numerical models from previous studies were simulated using the existing subroutine developed by Sandhaas [5] and the modified subroutine by Jayasekara and Foster [6], for standard and explicit analyses, respectively. This process enabled the development and application of a modelling methodology to simulate timber connections using validated subroutines.

Particularly for connection models where the complex demands on individual components, combined with their intricate interactions, necessitate careful consideration for the modelling methods discussed in the background section. In standard solution methods, the time step can be adjusted to refine the level of detail in the analysis output and control numerical instabilities caused by a large number of interactions. For explicit solution methods, defining an appropriate loading rate is essential, and mass scaling can be applied to improve control over time increments, minimising kinetic energy fluctuations within the finite element model.

The comparative analysis assessed the performance of available user subroutines for standard and explicit solution methods. In both cases, applying the crack band method reduced mesh dependency for elements under tensile stresses; however, for finer meshes, it introduced numerical instabilities. The explicit solver exhibited early failure, attributed to a brittle definition of shear and tensile stresses, especially in complex models where elements experienced multiple stress orientations.

The interaction between compression parallel to the grain, shear, and tension perpendicular to the grain significantly reduced the material's residual strength and transformed the expected plastic behaviour under compression into a brittle response. Additionally, the damage threshold parameter does not represent a physical material property, yet small variations significantly alter the entire response of the material model. The influence of fracture energy coefficients on model behaviour was minimal for the embedment test with the standard solver. It showed an average reduction of 5% of the strain energy; however, the overall impact of the fracture energy is highly dependent on the governing failure mode of the test. In scenarios where tensile or shear stresses predominantly drive failure, even minor variations in the fracture energy can modify the material response. Conversely, when compressive mechanisms parallel to the grain prevail, the sensitivity to these parameters appears considerably diminished.

These results emphasise the need to perform sensitivity analyses tailored to each failure mode and to calibrate the input parameters accordingly. Adjusting the modelling approach to reflect the primary failure mechanism can improve the accuracy of numerical predictions and provide better guidance in designing timber connections. For complex models, the explicit solver offers better computational efficiency; however, discrepancies were found in the Sandhaas subroutine when applied to explicit analysis, making standard analysis the preferred approach with the current subroutine.

ACKNOWLEDGMENT: This research was funded by the National Science Foundation (CMMI2046001).

6 – REFERENCES

[1] "Wood or Timber Market Size, Share, Growth, and Industry Analysis, By Type (Spruce, Pine, Beech Trees, Oak Trees, Eucalyptus, & Others), By Application (Wood-Working Industry, Furniture Industry, & Others), Regional Insights, and Forecast To 2032," Business Research Insights, Jan. 2025. [Online]. Available: https://www.businessresearchinsights.com/market-reports/wood-or-timber-market-108318

[2] J. L. Chaboche, "Continuum Damage Mechanics: Part I—General Concepts," *Journal of Applied Mechanics*, vol. 55, no. 1, pp. 59–64, Mar. 1988, doi: 10.1115/1.3173661.

[3] A. S. H. Makhlouf and M. Aliofkhazraei, Eds., *Handbook of materials failure analysis with case studies from the oil and gas industry*. Oxford, England: Butterworth-Heinemann, 2015.

[4] K. B. Dahl, "Mechanical properties of clear wood from Norway spruce," Norwegian University of Science and Technology, 2009.

[5] C. Sandhaas, "3D Material for Wood, based on Continuum Damage Mechanics User Subroutine UMAT," Delf University of Technology, Nov. 2011.

[6] L. M. M. B. Jayasekara and R. M. Foster, "Constitutive and numerical modelling for timber-metal connections under large deformations," *Engineering Structures*, vol. 315, p. 118462, Sep. 2024, doi: 10.1016/j.engstruct.2024.118462.

[7] C. Sandhaas, "Mechanical behaviour of timber joints with slotted-in steel plates," Delft University of Technology, Wohrmann, 2012.

[8] M. Gharib, A. Hassanieh, H. Valipour, and M. A. Bradford, "Three-dimensional constitutive modelling of arbitrarily orientated timber based on continuum damage mechanics," *Finite Elements in Analysis and Design*, vol. 135, pp. 79–90, Nov. 2017, doi: 10.1016/j.finel.2017.07.008.

[9] M. Wang, X. Song, and X. Gu, "Three-Dimensional Combined Elastic-Plastic and Damage Model for Nonlinear Analysis of Wood," *J. Struct. Eng.*, vol. 144, no. 8, p. 04018103, Aug. 2018, doi: 10.1061/(ASCE)ST.1943-541X.0002098.

[10] H. Eslami, L. B. Jayasinghe, and D. Waldmann, “Nonlinear three-dimensional anisotropic material model for failure analysis of timber,” *Engineering Failure Analysis*, vol. 130, p. 105764, Dec. 2021, doi: 10.1016/j.engfailanal.2021.105764.

[11] O. Hoffman, “The Brittle Strength of Orthotropic Materials,” *Journal of Composite Materials*, vol. 1, no. 2, pp. 200–206, Apr. 1967, doi: 10.1177/002199836700100210.

[12] F. Seeber, A. Khaloian-Sarnaghi, T. Yu, F. Duddeck, and J.-W. Van De Kuilen, “Development and validation of an orthotropic 3D elasto-plastic damage model for wood, considering fiber deviations,” *Engineering Structures*, vol. 308, p. 117928, Jun. 2024, doi: 10.1016/j.engstruct.2024.117928.

[13] M. Khelifa, A. Khennane, M. El Ganaoui, and A. Celzard, “Numerical damage prediction in dowel connections of wooden structures,” *Mater Struct*, vol. 49, no. 5, pp. 1829–1840, May 2016, doi: 10.1617/s11527-015-0615-5.

[14] R. Hill, “A theory of the yielding and plastic flow of anisotropic metals,” *Proc. R. Soc. Lond. A*, vol. 193, no. 1033, pp. 281–297, May 1948, doi: 10.1098/rspa.1948.0045.

[15] M. Mahendran, “Applications of Finite Element Analysis in Structural Engineering,” presented at the International Conference on Computer Aided Engineering, Queensland University of Technology, Australia, 2007.

[16] L. M. M. B. Jayasekara and R. M. Foster, “Numerical modelling of mass timber beam-column connections,” in *World Conference on Timber Engineering (WCTE 2023)*, Oslo, Norway: World Conference on Timber Engineering (WCTE 2023), 2023, pp. 2841–2850. doi: 10.52202/069179-0372.

[17] C. Sandhaas, A. K. Sarnaghi, and J.-W. Van De Kuilen, “Numerical modelling of timber and timber joints: computational aspects,” *Wood Sci Technol*, vol. 54, no. 1, pp. 31–61, Jan. 2020, doi: 10.1007/s00226-019-01142-8.

[18] M. Wang, X. Song, X. Gu, and J. Tang, “Bolted glulam beam-column connections under different combinations of shear and bending,” *Engineering Structures*, vol. 181, pp. 281–292, Feb. 2019, doi: 10.1016/j.engstruct.2018.12.024.

[19] A. Hassanieh, H. R. Valipour, M. A. Bradford, and C. Sandhaas, “Modelling of steel-timber composite connections: Validation of finite element model and parametric study,” *Engineering Structures*, vol. 138, pp. 35–49, May 2017, doi: 10.1016/j.engstruct.2017.02.016.

[20] C. J. Willmott *et al.*, “Statistics for the evaluation and comparison of models,” *J. Geophys. Res.*, vol. 90, no. C5, pp. 8995–9005, Sep. 1985, doi: 10.1029/JC090iC05p08995.

https://doi.org/10.52202/080513-0049